Numerical evaluation of the defrosting/defogging performance of HVAC system in the main product of the national vehicle platform

M.H. Shojaeefard[1]* , G.R. Molaeimanesh[2] , N. Aghamirzaei[3] , S. Ghezelbiglo[4] , B. Zeinolabedini[4]

1 Professor 2 Assistant professor and corresponding author 3 B.Sc. graduated in automotive engineering 4 M.Sc. automotive engineering student Automotive Engineering School, Iran University of Science and Technology,
* Corresponding Author

Abstract

Due to the increasing development in various branches of the automotive industry, the need for a comfort climate in the cabin is more sensible. However, to achieve climate comfort, HVAC system consumes a considerable amount of engine power. Hence, improving HVAC system performance leads to more energy saving of the vehicle which is a critical factor for nowadays automotive. Besides, one crucial task of HVAC system is defrosting/defogging of windshield which is considered as a mandatory requirement in most countries. In the current study, the defrosting/defogging performance of HVAC system in the main product of national vehicle platform is numerically evaluated based on the ECE-78-715 legal requirement. For this purpose, after validation and mesh independency study, the transient air flow in three-dimensional cabin geometry is simulated by SSTk-ω turbulence model via ANSYS Fluent software and the windshield thermal condition is reported during defrosting/defogging. Besides, two national HVAC standards of AERC-10-01 and AERC-10-02 are also checked. The results demonstrate that HVAC system of the main product of the national vehicle platform can satisfactorily fulfill ECE-78-715, AERC-10-01 and AERC-10-02.

Keywords*: defrosting/defogging performance; HVAC system; numerical evaluation; main product of the national vehicle platform; ECE-78-715.*

1. Introduction

Of the many demands placed on the automotive HVAC system, ensuring visibility through the windshield via defrosting/defogging is an important requirement for passenger safety [1]. Today's enhancing computing processors facilitates three-dimensional numerical simulation of a vehicle cabin to investigate different functions of HVAC system such as windshield defrosting/defogging. Several CFD assessments of different features of automotive air conditioning system have been carried out recently [2-8]. However, numerical evaluation of defrosting/defogging performance is not reported numerously; In fact, due to more reliability of experimental evaluation, automotive manufacturers preferred it to gain more ensuring about deicing capability of HVAC systems.

A numerical procedure for the prediction of transient defogging processes was described by Croce et al. [9]. The procedure computes the evolution of the water layer on an interface 2D grid, and the interaction with the flow solver is achieved through an exchange of boundary conditions. Thus, a high level of flexibility is granted, both in the choice of the flow solver and in the degree of interaction between the solver and the water layer routines.

Aroussi et al. presented a numerical model and technique to simulate the turbulent fluid flow over and heat transfer through a model of vehicle windshield defrosting and demisting systems [10]. The simplified geometry and the dimensions of the numerical model are representative of vehicle system with accurate locations of the nozzles and outlet vents, including cabin features such as seating and the rear parcel shelf.

The numerical results of their study compare favorably with measurements obtained from the actual vehicle by thermograph and hot bulb probe techniques. The findings highlight some of the drawbacks of the existing design of the windshield systems and show that the maximum flow rates occur in the vicinity of the lower part of the windshield, progressing from the defroster nozzle in the dashboard.

The windshield de-icing pattern analysis and windshield deicing process analysis have been discussed and validated by Farag and Huang [11]. Their results show reasonable agreement between the CFD prediction and the test results. They recommended to use the analysis in the early stages of the program to optimize the defroster nozzle design to shorten the development cycle. It is also recommended that the windshield de-icing pattern analysis be used during the refinement stage. The authors recommend a mesh size study to analyze the effect of the mesh size on the heat transfer calculations.

Kumara and Roy [12] investigated the unsteady process of melting of ice on the windshield using solidification and melting model, which relates enthalpy and porosity of ice, treated as mushy zone. The main goal of their paper was to compare the control parameters like impingement and sweep angle for minimization of defrosting time for a given ice and glass thickness. Parameters like enthalpy and Nusselt number are used to understand the heat transfer process. A comparative test using other viable alternatives deicing methods of deicing are also being attempted.

2. Governing equations

Computational fluid dynamics (CFD) is the science of predicting flow characteristics, mass and heat transfer, chemical reactions and other relating phenomena using numerical solutions to solve governing mathematical equations. These equations include conservation of mass (continuity law), conservation of momentum (Newton's second law), conservation of energy (first law of thermodynamics) and the conservation of chemical species. If the specific mass remains constant throughout the domain, the flow can be considered incompressible. Also the variation of viscosity can be ignored and taken to be a constant. Since the air flow through vehicle cabin can be considered incompressible, the governing equations in the averaged form are as follows:

a) Continuity equation:

$$\frac{\partial U_i}{\partial x_i} = 0 \qquad (1)$$

where U_i is the average velocity component in direction i.

b) Momentum equations:

$$\frac{\partial(\rho U_i)}{\partial t} + \frac{\partial(\rho U_i U_j)}{\partial x_j} = -\frac{\partial p}{\partial x_i} + \frac{\partial}{\partial x_j}\left[\mu_{eff}\left(\frac{\partial U_i}{\partial x_j} + \frac{\partial U_j}{\partial x_i}\right)\right] \qquad (2)$$

where P is pressure and μ_{eff} is the effective viscosity which equals:

$$\mu_{eff} = \mu_l + \mu_t \qquad (3)$$

Where μ_t is the turbulent viscosity and using the *SST k-ω* turbulent model, we can write:

$$\mu_t = \frac{a_1 \rho k}{\max(a_1 \omega, SF_2)} \qquad (4)$$

where S is strain rate and F_2 is:

$$F_2 = \tanh\left[\left[\max\left(\frac{2\sqrt{k}}{\beta^* \omega y}, \frac{500\nu}{y^2 \omega}\right)\right]^2\right] \qquad (5)$$

c) Turbulence equations [13,14]:

The transport equations for turbulence kinetic energy (k) and turbulence frequency (ω) are:

$$\frac{\partial k}{\partial t} + U_j \frac{\partial k}{\partial x_j} = P_k - \beta^* k\omega + \frac{\partial}{\partial x_j}\left[(\nu + \sigma_k \rho \mu_t)\frac{\partial k}{\partial x_j}\right] \qquad (6)$$

and

$$\frac{\partial \omega}{\partial t} + U_j \frac{\partial \omega}{\partial x_j} = \alpha S^2 - \beta \omega^2 + \frac{\partial}{\partial x_j}\left[(\nu + \sigma_\omega \rho \mu_t)\frac{\partial \omega}{\partial x_j}\right] + 2(1 - F_1)\sigma_{\omega 2}\frac{1}{\omega}\frac{\partial k}{\partial x_i}\frac{\partial \omega}{\partial x_i} \qquad (7)$$

where in Eqs. (6) and (7):

$$P_k = \min\left(\tau_{ij}\frac{\partial U_i}{\partial x_j}, 10\beta^* k\omega\right) \qquad (8)$$

and

$$F_1 = \tanh\left\{\left\{\min\left[\max\left(\frac{2\sqrt{k}}{\beta^* \omega y}, \frac{500\nu}{y^2 \omega}\right), \frac{4\sigma_{\omega 2} k}{CD_{k\omega} y^2}\right]\right\}^4\right\} \qquad (9)$$

where:

$$CD_{k\omega} = \max\left(2\rho\sigma_{\omega 2}\frac{1}{\omega}\frac{\partial k}{\partial x_i}\frac{\partial \omega}{\partial x_i}, 10^{-10}\right) \qquad (10)$$

The constants in the above equations are:

$$\alpha_1 = \frac{5}{9}, \quad \alpha_2 = 0.44 \qquad (11)$$

$$\beta_1 = \frac{3}{40}, \quad \beta_2 = 0.0828 \qquad (12)$$

$$\beta^* = \frac{9}{100} \quad (13)$$

$$\sigma_{k1} = 0.85, \quad \sigma_{k2} = 1 \quad (14)$$

$$\sigma_{\omega 1} = 0.5, \quad \sigma_{\omega 2} = 0.856 \quad (15)$$

2. Numerical Method

To numerically solve the governing equations in a physical domain, one of the three methods below is chosen:

Finite difference method
Finite volume method
Finite element method

Due to its more flexibility, finite volume method is usually adopted for solving fluid flow in a computational domain. In this method, the integral forms of conservation equations are solved for the finite control volumes adjacent to each other. Finite volume method is able to handle a variety of complex geometry problems. ANSYS Fluent software which is used in the current study is based on the finite volume method.

In most engineering problems where natural convection cannot be neglected, to estimate the variations of density with temperature with a high convergence rate the Boussinesque approximation method [15] can be used. In this method, it is assumed that the density of the fluid remains constant in all governing equations, except in the volumetric force term in the momentum equation in the direction of the gravity which is:

$$(\rho - \rho_0)g = -\rho_0 \beta (T - T_0)g \quad (16)$$

Where T0 is the reference temperature, ρ0 is the flow density at T0 (constant), and β is the thermal expansion coefficient. The thermal expansion coefficient is set at 0.00335 in the current software.

3.1. Turbulent Model

In this study, the SST k-ω turbulent model is used due to its high performance capability in flow simulations in a wide range of Reynolds number and also a relatively low computational cost for simulation of turbulence. SST k-ω turbulence model which is a two-equation Reynolds averaged Navier-Stokes (RANS) turbulence model [16] has advantageous features such as high prediction capability, economical factor and more important than anything else, acceptable accuracy in a wide range of turbulence flows. This model is widely used in engineering fluid flows including reverse pressure gradient, airfoils and transient shock waves.

SST k-ω turbulence model is quite suitable for boundary layer flows where it performs better than the well-known k-ε model. In most of two-equation models such as the k-ε turbulence model, turbulent stress at the wake vicinity is over estimated, which leads to weak performance. The main idea if SST k-ω turbulence model is the combination of the capability of the so-called k-ω turbulence in predicting flow field near the solid boundary with the capability of k-ε turbulence model in predicting high-Reynolds number flow far away from the solid boundary.

3.2. Model Validation

In order to validate the employed software for the simulation, it is necessary to compare the numerical results with experimental data. The experimental data adopted for validation belong to the two-dimension simulation of Nielsen et al. [17] which is widely used for validation of internal flow. The Nielsen et al. flow field is shown in Fig.1 in which the Reynolds number based on the inlet characteristics is set to 5000.

The experimental data and the results of numerical simulation via ANSYS Fluent are compared in two horizontal lines of $\frac{y}{H} = 0.028$ and $\frac{y}{H} = 0.972$; and the two vertical lines of $\frac{x}{L} = \frac{1}{3}$ and $\frac{x}{L} = \frac{2}{3}$ in Fig2 and Fig3, respectively. As it is obvious, the difference of experimental data and the numerical results is acceptable.

4. Computation domain

The interior geometry of the main product of the first national vehicle platform is modeled via CATIA software. In order to reduce computational cost, details of the interior have been neglected due to their small effects on the outcome. It should be noted that the cabin geometry considered in this simulation is the volume inside the cabin containing fluid, from which the volume of components such as the front or rear row passenger seats is subtracted. In Fig.4 (b) different parts of the model (seats, front and rear air vents (registers), center console, parcel shelf, windows, dashboard, roof, floor, firewall and doors) are shown.

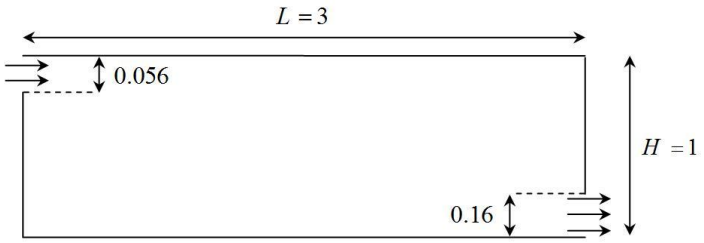

The geometry of model studied experimentally by Nielsen et al. [17]

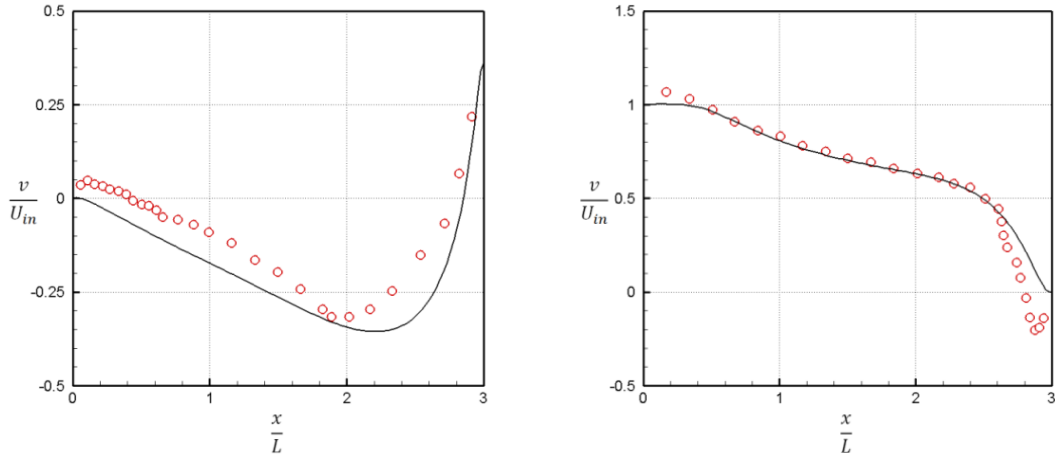

(a) $\frac{y}{H} = 0.028$ (b) $\frac{y}{H} = 0.972$

. Comparison of the numerical results with the experimental data from Nielsen et al. [17] for two horizontal lines (symbols: experimental data; solid line: the results of the present numerical study)

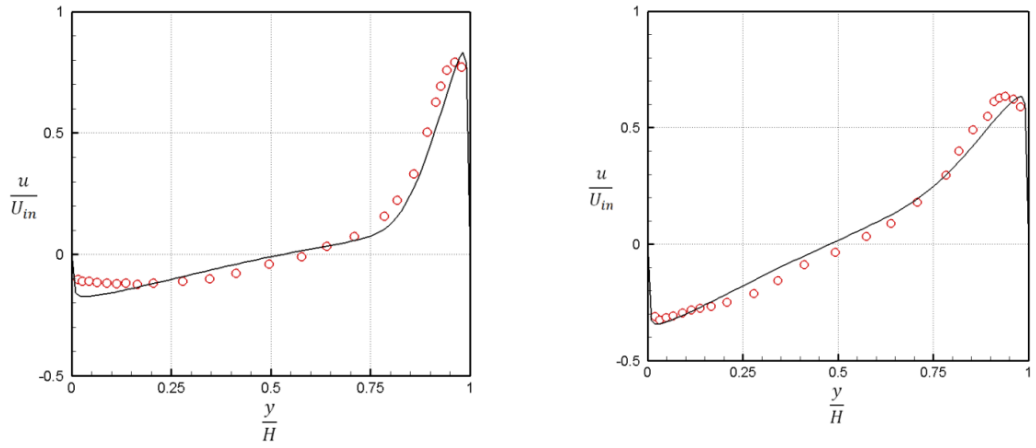

(a) $\frac{x}{L} = \frac{1}{3}$ (b) $\frac{x}{L} = \frac{2}{3}$

Comparison of the numerical results with the experimental data from Nielsen et al. [17] for two vertical lines (symbols:

experimental data; solid line: the results of the present numerical study)

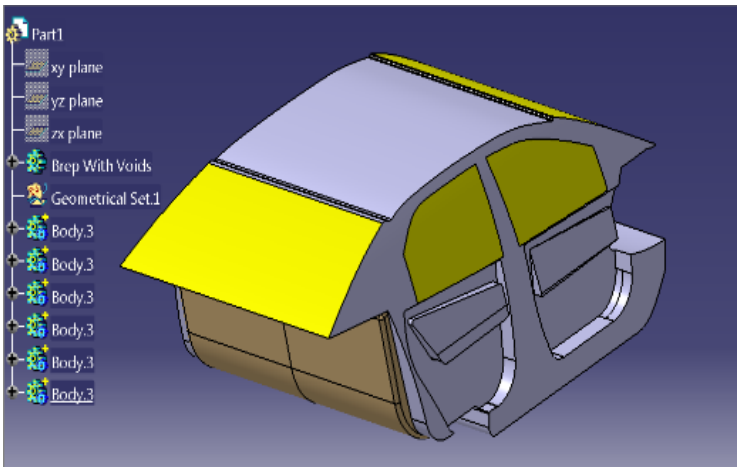

(a) Outer view

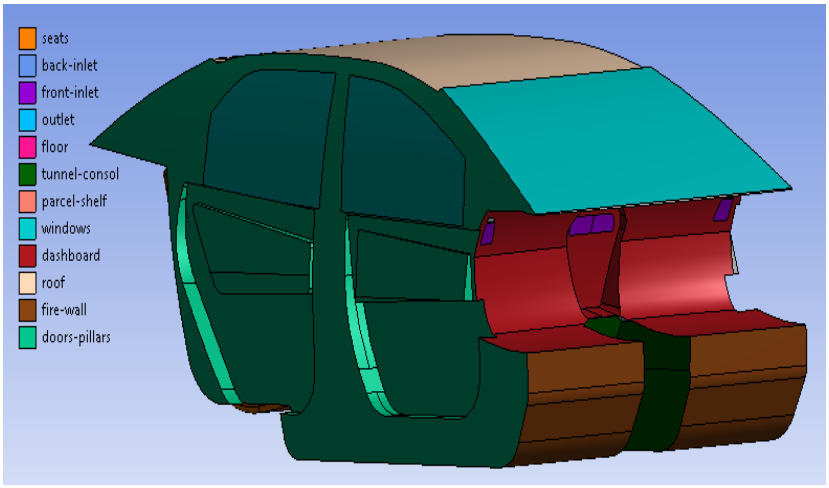

(b) Inner view

Fig4. The geometry of computational domain

An unstructured tetrahedral mesh is generated for simulation of air flow in the computational domain which can be seen in Fig. 5. The generated mesh consists of approximately 1.4 million cells using path conforming algorithm. It contains an average aspect ratio of 1.8 and an average skewness of 0.23. The maximum acceptable value for aspect ratio and skewness is 5 and 0.33, respectively [18]. Their ideal values are 1 and 0, respectively.

It is necessary to mentioned that the afore-mentioned 1.4 million of cells is based on a mesh independency study performed. In such a study, various meshes with different number of cells are simulated and the results are compared. There would be an optimum number of cells that using less number of cells could lead to incorrect results while applying greater number of cells could lead to unnecessary extended computational cost without any significant accuracy improvement.

In order to achieve this optimum number, several meshes have been simulated and the average air temperature is reported as the determinative parameter. In these simulations, the rear air vent on the parcel shelf is opened to atmosphere while cool air enters through the front and rear air registers with the uniform velocity of 1.6 m/s.

The results can be seen in Table 1.

According to above statistical results, the variation of cabin temperature for 1.4 million cells or more is below 2.5%. Therefore in the following sections, the number of cells used is set to 1.4 million. Other parameters settings applied in the simulations are presented in Table 2.

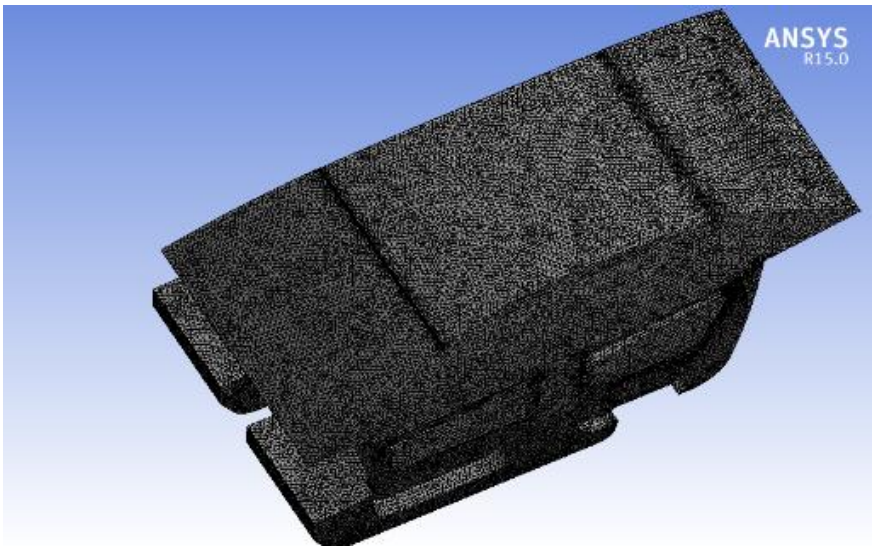

(a) Isometric view

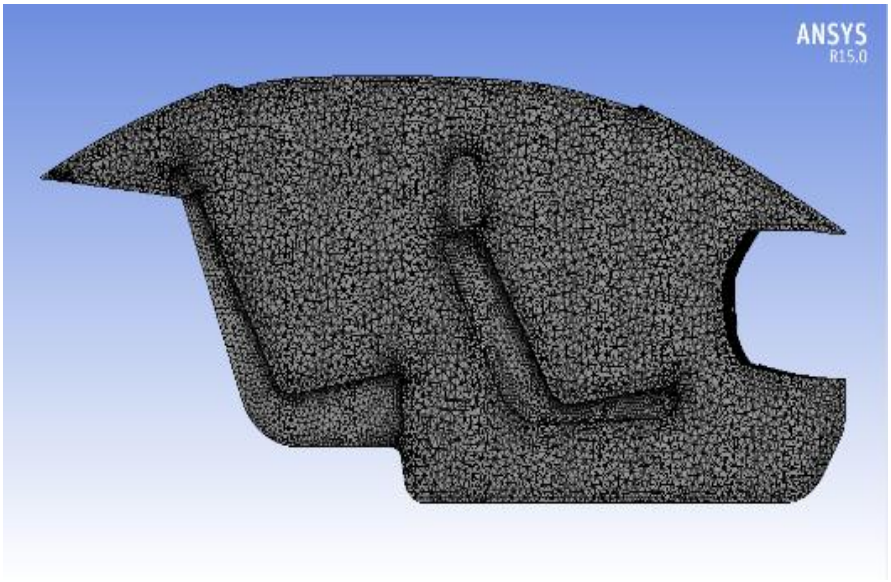

(b) Cross section view

Fig.5 the mesh generated for numerical simulation

Table 1- Variation of the average cabin temperature (°C) vs. number of cells in the mesh independency study.

Number of meshes	2,000,000	1,700,000	1,400,000	1,200,000	1,000,000	700,000
Average cabin temperature	27.08	26.33	27.01	27.15	26.83	25.76

Table 2- Parameters settings applied in the current simulations.

Operating Conditions	
Operating Pressure	101325 Pa
Gravity	Enabled
Bossiness Parameter (operating temperature) [K]	288.16
Variable density parameter	Enabled
Solar Load Model	
Model	Do Irradiation
Diffuse Solar Irradiation	Constant (200)
Direct Solar Irradiation	Solar-Calculator
Global Position	Longitude=31.2 Latitude=48.4 Time zone(GMT)=4.5
Date and Time	Day=23 Month=7 Time=13:00
Solar Irradiation Method	Fair Weather Condition
Sunshine Factor	1
Pressure-Velocity Coupling	
Model	SIMPLE
Boundary Conditions	
Dashboard Inlets	
Type	Velocity-Inlet
Turbulence	Intensity and Hydraulic Diameter
Turbulent Intensity	5%
Hydraulic Diameter	Side: 0.07 Middle: 0.08
Temperature [K]	Variable in different simulations
Back Inlet	
Type	Velocity-Inlet
Velocity specification Method	Intensity and Hydraulic Diameter
Velocity Magnitude	Magnitude and Direction
Direction X Component	0.7071
Direction Y Component	0
Direction Z Component	0.7071
Turbulent Intensity	5%
Hydraulic Diameter	0.075
Temperature	Variable in different simulations
Outlet	
Type	Pressure Outlet
Gauge Pressure	0(Constant)
Backflow Total Temperature [K]	300
Turbulent Specification Method	Intensity and Hydraulic Diameter
Backflow Turbulent Intensity	5%
Hydraulic Diameter	0.05

5. Results and discussion

5.1. Air conditioning defrosting/defogging performance evaluation

The conducted transient simulations based on 78-318-EEC standard for different initial temperatures and different time settings are presented in this section. At first, defogging process is elucidated. The titles of following subsections, (a) till (e), which are according to different requirements of 78-318-EEC represent the simulations performed.

Defogging of zone A of front windshield at environment temperature of -3 °C after 5 minutes

In this state, the initial temperature of the front windshield and all other cabin components is set at -3 °C. The temperature distribution contour on the windshield after 5 minutes is shown in Fig6. As it can be seen, the temperature of windshield on zone A (the two trapezoidal shapes marked in this figure) is above 0 °C which shows the ability of the designed HVAC system in satisfying this requirement.

Defogging of the entire front windshield at environment temperature of -3 °C after 11 minutes

Shown in Fig7 is the temperature distribution contour on the windshield after 11 minutes. As it is obvious, the temperature of windshield is entirely above 0 °C which shows the ability of the designed HVAC system in satisfying this requirement.

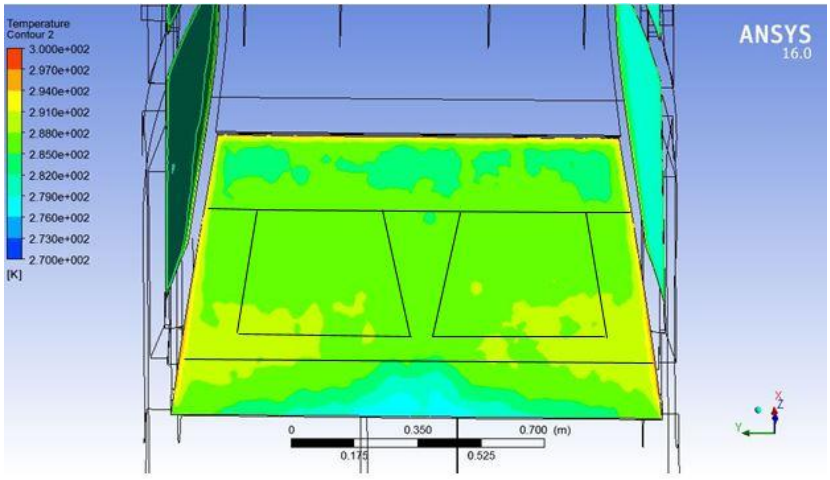

Fig6. Defogging of zone A of front windshield at environment temperature of -3 °C after 5 minutes

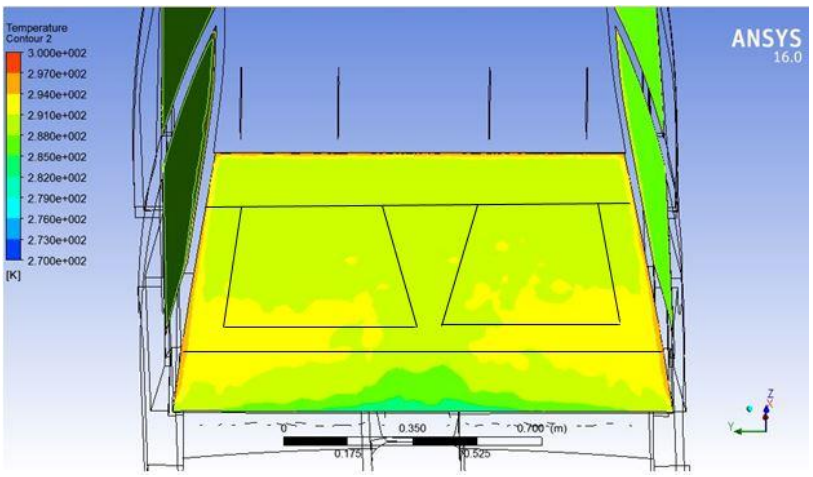

Fig7. Defogging of the entire front windshield at environment temperature of -3 °C after 11 minutes

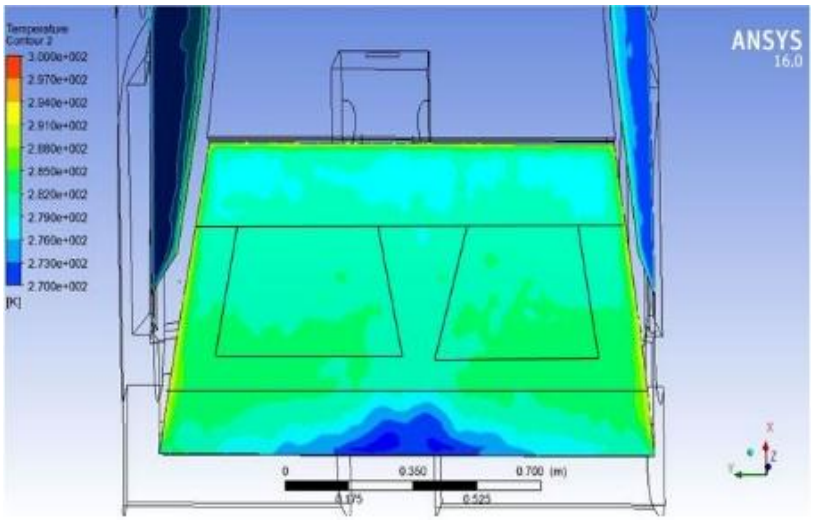

Fig8. Defrosting of zone A of front windshield at environment temperature of -8 °C after 15 minutes

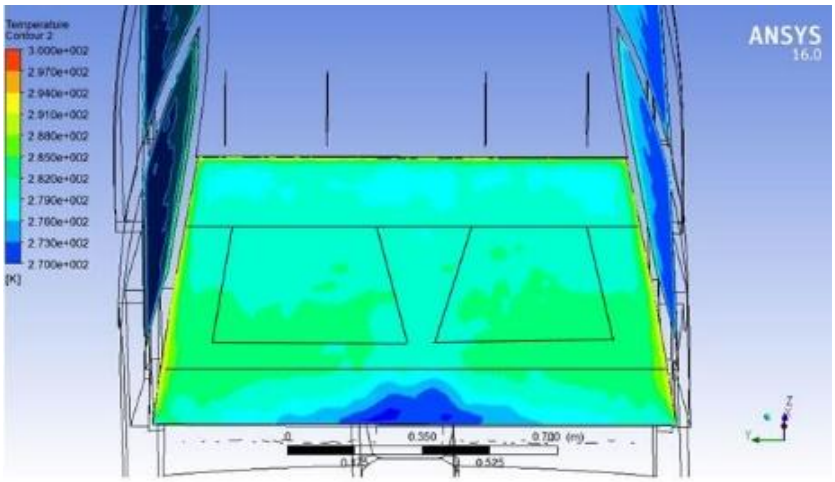

Fig9. Defrosting of the entire front windshield at environment temperature of -8 °C after 25 minutes

Defrosting of zone A of front windshield at environment temperature of -8 °C after 15 minutes

In this state, the initial temperature of the front windshield and all other cabin components is set at -8 °C. The temperature distribution contour on the windshield after 15 minutes is shown in Fig8. As it can be seen, the temperature of windshield on zone A (the two trapezoidal shapes marked in this figure) is above 0 °C which shows the ability of the designed HVAC system in satisfying this requirement.

Defrosting of the entire front windshield at environment temperature of -8 °C after 25 minutes

Shown in Fig9 is the temperature distribution contour on the windshield after 25 minutes. As it is obvious, the temperature of windshield is entirely above 0 °C which shows the ability of the designed HVAC system in satisfying this requirement.

As the numerical results in the above four subsections established, the designed HVAC system for the main product of the national vehicle platform can fulfill the mandatory requirement of 78-318-EEC.

5.2. Thermal comfort evaluation

In order to check the performance of the air conditioning system in providing a thermally comfortable environment for the passengers, two optional requirements of AERC-10-01 and AERC-10-02 are also used for evaluation.

AERC-10-01

AERC-10-01 is introduced by automotive engineering research center (AERC) in the Iran University of Science and Technology to evaluate the heating performance of the HVAC unit. In this requirement, the initial cabin temperature is set at -20 °C. After initiating the heating operation of the HVAC unit, the following demands should be satisfied:

A) The average cabin temperature after 15 minutes while the vehicle running at 40 km/h should reach 15 °C.

B) The air temperature at the exhaust vent after 15 minutes while the vehicle running at 40 km/h should reach 13.9 °C.

C) The average cabin temperature after 30 minutes while the vehicle running at 40 k/ph should reach 29 °C.

D) The air temperature at the exhaust vent after 30 minutes while the vehicle running at 80 km/h should reach 34°C.

E) The air temperature at the exhaust vent while the vehicle is running at a constant speed of 80 km/h and after 10 minutes of idle should reach 32 °C.

The numerical results demonstrate that all the above mentioned criteria can be passed via the designed HVAC system for the main product of the first national platform. In fact, the average air temperature of the cabin after 15 minutes, reaches 19.5 °C which is well beyond the 15 °C which confirms the flawless performance of the designed heating unit.

AERC-10-02

According to this criterion which is introduce by AERC to evaluate the cooling capability of a HVAC system, the initial cabin temperature is taken to be 52 °C. After initiating the cooling operation of the HVAC unit, the following demands should be satisfied:

A) The average cabin temperature after 15 minutes while the vehicle running at 40 km/h should reach 29 °C.

B) The air temperature at the discharge vent after 10 minutes while the vehicle running at 40 km/h should reach 20.6 °C.

C) The average cabin temperature after 30 minutes which the vehicle running at 40 km/h should reach 26 °C.

D) The air temperature at the discharge vent after 30 minutes while the vehicle running at 80 km/h should reach 25 °C.

E) The air temperature at the discharge vent while the vehicle is running at a constant speed of 80 km/h and after 30 minutes of idle should reach 26 °C.

The numerical results demonstrate that all the above mentioned criteria can be passed via the designed HVAC system for the main product of the first national platform. In fact, the average air temperature of the cabin after 15 minutes, reaches 28.33 °C which is well beyond the 29 °C which confirms the acceptable performance of the designed heating unit.

6. Conclusions

One of the main functions of an air conditioning unit which is of great importance is defogging/defrosting ability which is considered as a mandatory requirement in many countries. The design of the defogger and defroster depend on many factors including the design of air ducts, air temperature, air speed and turbulence level.

In this study, the capability HVAC system designed for the main product of the national vehicle platform in defrosting/defogging of windshield is numerically evaluated by ECE-78-715 standard. The air flow inside the cabin is simulated three-dimensionally using ANSYS Fluent and via the SST k-ω turbulent model. In this regard, validation and mesh independency study are performed at first. The results of simulations demonstrate that the designed HVAC system for the main product of national vehicle platform can fulfill the legal defrosting/defogging requirement of 78-318-EEC. Besides, to confirm the HAVC system capabilities in providing thermal comfort, the heating and cooling performances are evaluated via AERC-10-01 and AERC-10-02 criteria, respectively which were successfully established.

Reference

[1]. Kye-Kwangand, Choi, and Han Seong-Ryeol. "Numerical Study for Connecter and Section Shape of the Internal Heat Exchanger on Automotive Air Conditioning." *Indian Journal of Science and Technology* 8.S8 (2015): 144-148.

[2]. Lee, G. H., and J. Y. Yoo. "Performance analysis and simulation of automobile air conditioning system." *International journal of refrigeration* 23.3 (2000): 243-254.

[3]. Danca, Paul, Andreea Vartires, and Angel Dogeanu. "An Overview of Current Methods for Thermal Comfort Assessment in Vehicle Cabin." *Energy Procedia* 85 (2016): 162-169.

[4]. Kader, MD Faisal, Mohammad Ali Jinnah, and Kumbae Lee. "the effect of solar radiation on automobile environment through natural convection and mixed convection." *Journal of Engineering Science and Technology* 7.5 (2012): 589-600.

[5]. R. Gordon, M. Imbabi, CFD simulation and experimental validation of a new closed circuit wind/water tunnel design, J. Fluids Eng. Trans. ASME 120 (1998) 311-318.

[6]. R.H. Vaivads, D. Springford, G. Lemieux, J.E.D. Gauthier, in: CFD Simulation of Turbulence Reduction in a Wind Tunnel Using Screens, the 1997 ASME Fluids Engineering Division Summer Meeting, June 1997, pp. 1-5.

[7]. D.C. Cumberpatch, Climatic simulation in a purpose-built wind tunnel, Proc. Inst. Mech. Engrs., I Mech. E 201 (D4) (1987).

[8]. Ghani, SAA Abdul, A. Aroussi, and E. Rice. "Simulation of road vehicle natural environment in a climatic wind tunnel." simulation practice and theory 8.6 (2001): 359-375.

[9]. Croce, G., et al. "A numerical procedure for defogging process simulation in automotive industry." International Conference on Heat and Mass Transfer, Corfu, Greece, August. 2004.

[10]. Aroussi, A., A. Hassan, and Y. Morsi. "Numerical simulation of the airflow over and heat transfer through a vehicle windshield defrosting and demisting system." Heat and Mass Transfer 39.5-6 (2003): 401-405.

[11]. Farag, Ashraf, and Lin-Jie Huang. "CFD Analysis and Validation of Automotive Windshield De-Icing Simulation." SAE paper 2003-01 (2003): 1079.

[12]. Kumar, Haribalan, and Subrata Roy. "Improved de-icing of an inclined windshield surface." 43rd AIAA Aerospace Sciences Meeting and Exhibit. 2005.

[13]. Menter, F. R. (1993), "Zonal Two Equation k-ω Turbulence Models for Aerodynamic Flows", AIAA Paper 93-2906.

[14]. Menter, F. R. (1994), "Two-Equation Eddy-Viscosity Turbulence Models for Engineering Applications", AIAA Journal, vol. 32, no 8. pp. 1598-1605.

[15]. Incropera F.P., DeWitt D.P., Bergman T.L., Lavine A.S. (2007). Fundumentals of Heat and Mass Trandfer, John Wiley and Sons, New Jersey.

[16]. Wilcox D. C., "Turbulence Modeling for CFD", DCW Industries, Inc., 1993.

[17]. Nielsen, P.V., Restivo, A., Whitelaw, J.H., .The velocity characteristics of ventilated rooms, Journal of Fluid Engineering, Vol.100, pp.291-298, 1978.ANSYS User's guide, R15.01.